A Tryptophan Rotamer Located in a Polar Environment Probes pH-Dependent Conformational Changes in Bovine β-Lactoglobulin A

Billie J. Harvey, Erin Bell, and Lorenzo Brancaleon*

Department of Physics and Astronomy, University of Texas at San Antonio, San Antonio, Texas

Received: September 5, 2006; In Final Form: January 7, 2007

Bovine β-lactoglobulin A (BLGA) is a well characterized globular protein whose tertiary structure has been investigated in detail. BLGA undergoes a pH-dependent conformational change which X-ray data described as involving mostly the loop connecting strands E and F and the deprotonation of a glutamic acid residue (Glu89). These structural changes have been investigated using, among other techniques, fluorescence spectroscopy. The intrinsic fluorescence of BLGA is dominated by two Trp residues. These residues are located far from the EF loop and would not be expected to probe the pH-induced conformational change of the protein. Trp19 is located at the bottom of the interior β-barrel, whereas Trp61 is located at the aperture of the barrel near the CD loop and is "silent" in the emission of native BLGA because of the proximity of a disulfide moiety. Our study suggests that, surprisingly, the fluorescence of Trp19 has the characteristic of a more polar environment than structural models from X-ray data would suggest and that at least two distinct conformations (or rotamers) of Trp19 contribute to the fluorescence of the protein. The less populated rotamer (relative amplitude (α) ∼20%, $\tau \sim 3$ ns) probes a more polar environment and a pH-dependent conformational change of BLGA in the region of Trp19 which X-ray data do not detect. Finally, our study provides the estimate of the fluorescence lifetime of Trp61 in the "unquenched" form.

Introduction

The photophysical properties of bovine β-lactoglobulin (BLG) have been investigated for several decades, as they can be used to study the structural properties of native and mutated BLG[1−7] as well as characterize the interaction of the protein with ligands and smaller macromolecules.[8−14] In addition, since BLG structural data are very extensive,[15,16] the protein represents an appealing model to correlate local conformational changes with optical properties such as fluorescence,[5,17,18] circular dichroism (CD),[3,19,20] infrared,[4,21] and Raman spectroscopy.[7] BLG (both variants A and B) can be summarized as a small globular protein of 162 amino acids (Figure 1) whose main structural feature is an interior β-barrel formed by eight β-strands, intersecting almost orthogonally.[15,16] X-ray diffraction indicates that the loop connecting strands E and F (EF loop) is the major region responsible for the conformational change occurring around pH 7.5.[15] A three-turn α-helix flanks one side of the calyx and is involved in the formation of the BLG dimer[15,16] (Figure 1). In addition, a 3_{10} helix, in the most conserved region of the lipocalins,[15,16] "closes" the barrel at the bottom.

Despite the detail, the high resolution structural data fail to explain some of the experimental evidence obtained in solution such as the pH-dependent reactivity of the lone free cysteine (Cys121)[19,22,23] and the fluorescence quenching by acrylamide.[24] It is therefore conceivable that the pH-induced conformational changes of the protein in aqueous solution, at the micromolar range, could introduce changes that may go undetected in X-ray. A survey of available structures (PDB files 1UZ2, 1BSY, 2BLG, 3BLG, 1BSQ, and 1BSO) reveals that the overall B-factor for BLG is 45.2 ± 10 which is relatively high[25−28] and that some regions, although buried, are quite mobile. In the 3−9 pH range, bovine β-lactoglobulin A (BLGA) in solution is a homodimer.[20,29] The dimer is stabilized by hydrogen bonds between strand I in each protein as well as the opposite charges at the end of the major α-helix.[16]

The two monomers can be separated, without causing major conformational rearrangements, using denaturants (urea) or temperature.[5,30] Such dissociation might be relevant to rationalize the interaction of BLG with some ligands. The location and role of the suggested binding sites is still controversial and includes (i) the interior barrel,[1,8,29] (ii) a "superficial" binding site formed between the three-turn α-helix and the exterior portions of strands I, G, H, and A,[9,14,16,29,31] and (iii) binding sites created at the monomer/monomer interface.[13,31]

Since binding to various ligands is one of the issues important to revealing the still unclear function of this protein, fluorescence spectroscopy has been used extensively to investigate the interactions of BLG with other molecules using both exogenous dyes[9,10,13] and intrinsic fluorescence.[1,8,32]

Despite its widespread use, the detailed description of the intrinsic properties of BLG emission is still controversial. BLGA contains four tyrosine (Tyr) residues in positions 20, 42, 99, and 102 and two tryptophan residues (Trp) in positions 19 and 61.[16,29] A survey of the available BLGA structures at the Protein Data Bank shows that Tyr residues 20, 99, and 102 are clustered within 9 Å of Trp 19, whereas Tyr 42 is approximately 11 Å from Trp 61. These distances are well short of the 17 Å estimated as Forster's radius for the energy transfer between the phenol and the indole group.[33] Thus, a strong Tyr → Trp energy transfer and/or static quenching[34,35] of Trp on Tyr residues is expected and the intrinsic emission of BLG is dominated by Trp residues.[24] Nonetheless, opposite interpretations on the contribution of Trp19 and Trp61 BLG emission have been suggested. We believe that the experiments of Cho

* Address correspondence to: Department of Physics and Astronomy, University of Texas at San Antonio, One UTSA Circle, San Antonio, Texas 78249.

10.1021/jp065783a CCC: $37.00
Published on Web 02/15/2007

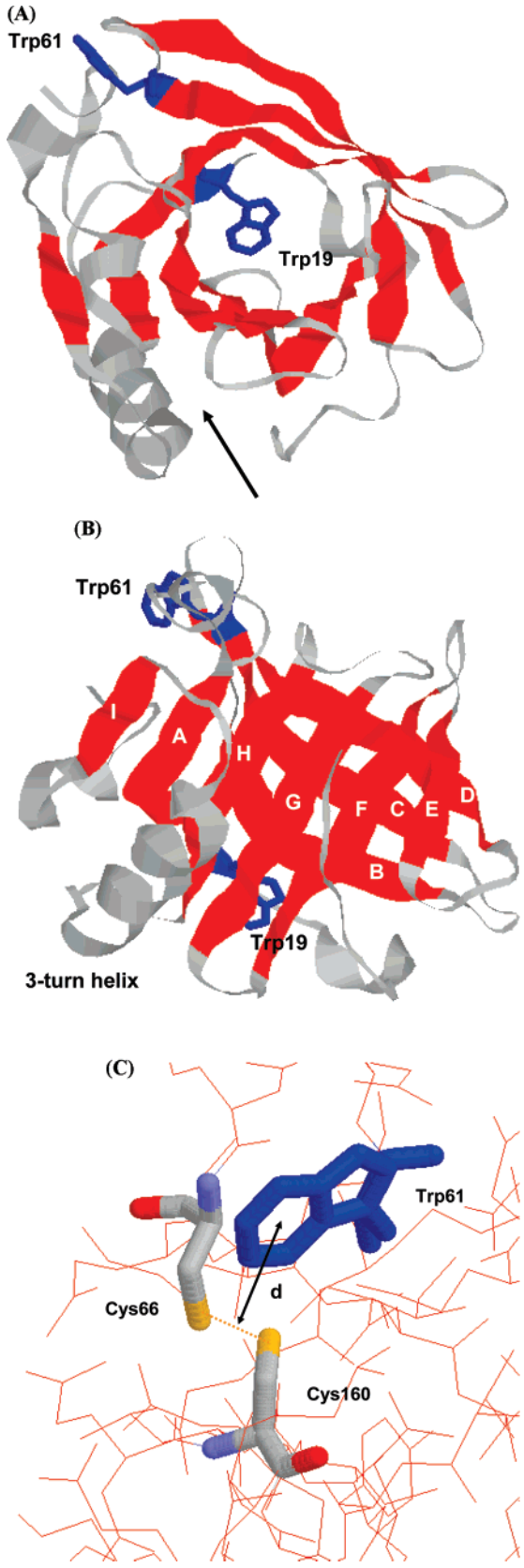

Figure 1. (A) Overall structure of BLG (from PDB file 1B08). The view is from the top of the interior β-barrel looking down into it. The barrel is often indicated as the main binding site for hydrophobic molecules. The two Trp residues are visualized with Trp19 at the bottom of the barrel, and the arrow indicates a possible alternative binding site. (B) Side view of BLG with the Trp residues still visualized. Each β-strand is labeled. In parts A and B, the β-strands are represented in red and the Trp residues in blue. (C) View of Trp61 and its proximity ($d \sim 3.7$ Å) to the Cys66−Cys160 disulfide moiety.

et al.[8] indicate that the contribution of Trp61 to the fluorescence of native BLG is negligible. On the basis of this conclusion, questions remain regarding the properties of the Trp19 fluorescence. A thorough characterization of Trp19 contribution is therefore extremely important to the interpretation of fluorescence data. Trp 19 is located at the bottom of the calyx in what X-ray data indicate as a very hydrophobic region,[15,16] while Trp 61 is located near the aperture of the barrel with the indole ring pointing away from the aperture which renders this residue more exposed to the aqueous solvent (Figure 1). Moreover, Trp61 is in proximity (3.5−3.8 Å) of the Cys66−Cys160 disulfide bridge (Figure 1C) which is a strong quencher of indole fluorescence.[17,19,22,34,36,37]

We initiated this study to better characterize the contribution of the two Trp residues to the overall emission of the protein and in the process improve the interpretation of binding data reported by our group and others (see references above).

Our results reveal that, although located in a hydrophobic pocket, Trp19 is exposed to interactions with residues that produce fluorescence features more characteristic of a polar environment. The emission wavelength, the emission lifetimes, and the dependence of the fluorescence decay on the emission wavelength are in fact more in agreement with Trp residues in some degree of polar and/or inhomogeneous environments.[38] Such behavior has been observed in other proteins and peptides.[35,37,39]

Experimental Methods

Chemicals. BLGA (L-7880, Sigma-Aldrich, St. Louis, MO) was >99% pure (as assessed by SDS-PAGE and HPLC) and was thus used as received. Urea (Fluka 51459, Sigma-Aldrich, St. Louis, MO), *N*-acetyl-L-tryptophanamide (NATA) (A6501, Sigma-Aldirch, St. Louis, MO), KI (Fluka 60399, Sigma-Aldrich, St. Louis, MO), and acrylamide (A-3553, Sigma-Aldrich, St. Louis, MO) were also used as received. Buffers (10 mM) were prepared by dissolving one pellet of phosphate buffered saline (P4417, Sigma-Aldrich, St. Louis, MO) in 200 mL of water purified by reverse osmosis (Diamond RO, Barnstead, Dubuque, IA). The final pH value of the buffer was adjusted by adding small aliquots of a 0.5 N HCl solution or 1 M NaOH solution.

Experimental Conditions. At all pH values, BLGA was dissolved directly in buffer at a concentration of ~6 μM. This concentration was chosen to ensure that the optical density at the excitation wavelength remained between 0.05 and 0.1. The 10 mM phosphate buffers were prepared from pH 5 to pH 9 at increments of one unit.

For denaturation experiments, samples were prepared by adding the solid urea directly in solutions containing BLGA for a final denaturant concentration range of 1−8 M at increments of 1 M. The same method was used at each pH.

For quenching experiments, various aliquots of KI or acrylamide, from a 1 M stock solution at the appropriate pH, were added to 1.5 mL of solution containing BLGA. The concentration range for both quenchers was 0.0−0.3 M.

Fluorescence Spectroscopy. Emission spectra were recorded using a double-monochromator AB-2 fluorimeter (Thermoelectron, Madison, WI). Intrinsic emission, as well as excitation, fluorescence spectra of BLGA and NATA were initially recorded. Emission spectra recorded with 280 or 295 nm were identical, after normalization for the optical density at the excitation wavelength. Excitation spectra were recorded at several fixed emission wavelengths from 320 to 380 nm at increments of 10 nm. All spectra, after normalization of the

emission intensity, overlapped (data not shown). The evidence above strongly supports the assumption that the intrinsic fluorescence of BLGA is due to Trp residues. The optical density of the solution at the excitation wavelength was kept near 0.1 and was measured using a dual-beam spectrophotometer (Evolution 300, Thermoelectron, Madison, WI). All experiments were carried out using 1 cm path length quartz cells (Sigma-Aldrich, St. Louis, MO, and Starna Cells Inc., Atascadero, CA). Emission spectra were recorded in the 300−450 nm range. Acquisition of the spectra was carried out using a 4 nm bandpass in both the excitation and emission monochromator.

Fluorescence Decay. Intrinsic fluorescence decay lifetimes were measured with a time-correlated single photon counting (TCSPC) instrument (IBH 5000 U, JobinYvon, Edison, NJ), using a sub-nanosecond 280 nm pulsed LED (NanoLED-15, pulse width ≈700 ps, IBH Ltd., Glasgow, U.K.) at a 1 MHz repetition rate. Fluorescence decays were accumulated at a counting rate of <20 000 counts/s up to a 10 000 peak count at various emission wavelengths from 300 to 400 nm. The temporal resolution was maintained at 57 ps/channel, and the decay window was 58 ns. The slits on the excitation monochromator were set at 4 nm (consistent with the steady-state settings). With all samples, fluorescence decay experiments were carried out immediately after the steady-state experiments on the very same solutions. For each decay curve, a "prompt" decay was recorded using a scattering solution of 0.1 mg/mL glycogen in buffer. The word "prompt" represents the instrument response function, $G(t)$ (see below), or, in other words, the time profile of the pulsed source.

All fluorescence experiments were repeated in triplicate, and the average was used for data analysis.

Fluorescence Intensity Data Analysis. Emission intensity was normalized for the optical density of the samples at 280 nm (and 295 nm), and fluorescence intensity was calculated as the area of the emission spectrum calculated from 300 to 450 nm.

Stern−Volmer (S−V). We used the classic S−V plots[40] to describe the quenching of BLG intrinsic fluorescence upon addition of KI or acrylamide. S−V theory predicts that in the case of collisional quenching, such as the case for KI and acrylamide, the relative decrease of the fluorescence intensity depends linearly on the concentration of the quencher.

$$\frac{F_0}{F} = 1 + K[\mathrm{Q}] = \frac{\tau_0}{\tau} \tag{1}$$

where F_0 is the starting, normalized fluorescence intensity in the absence of quencher and F is the normalized fluorescence intensity in the presence of a concentration of quencher, [Q]. K is the quenching constant. Deviation from linearity normally occurs at high [Q];[40] however, within a certain initial range, S−V plots can be considered linear.[40]

Addition of Urea. The changes in the emission of BLGA and NATA upon addition of urea were analyzed by using the model presented by Galani and Apenten.[5] The model assumes that the addition of urea produces the unfolding of BLGA through an intermediate state that forms through the dissociation of the dimer into two monomers that retain their tertiary structure (dissociation coupled unfolding or DCU).

Briefly, the free energy change associated with the denaturant-induced unfolding is

$$\Delta G_{\mathrm{DCU}} = \Delta G^{\circ}_{\mathrm{DCU}} - m[\mathrm{D}] \tag{2}$$

where $\Delta G^{\circ}_{\mathrm{DCU}}$ is the free energy change for the unfolding reaction in the absence of denaturant at $T = 20$ °C defined according to Galani[5] and m is a denaturant index.[41]

Under the conditions of our experiments, the fluorescence at each concentration of urea can be represented as

$$F_{\mathrm{DEN}} = \frac{F - F_{\mathrm{MAX}}}{F_{\mathrm{MAX}} - F_{\mathrm{MIN}}} \tag{3A}$$

where F is the fluorescence of BLG at a given urea concentration, F_{MAX} is the maximum fluorescence which occurs at 8 M urea, and F_{MIN} is the minimum fluorescence at 0 M urea.[5] ΔG_{U} is determined by

$$\Delta G_{\mathrm{U}} = -RT \ln K_{\mathrm{U}} \tag{3B}$$

and assuming that, for the DCU model, K_{U} is represented by[5]

$$K_{\mathrm{U}} = 4[\mathrm{BLGA}]\frac{(F_{\mathrm{DEN}})^2}{1 - F_{\mathrm{DEN}}} \tag{3C}$$

where [BLGA] is the concentration of lactoglobulin which for our samples was maintained constant at 6 μM.

This model was compared with the classic two-state (TS) model which instead predicts that K_{U} is described according to

$$K_{\mathrm{U}} = \frac{F_{\mathrm{DEN}}}{1 - F_{\mathrm{DEN}}} \tag{3D}$$

Fluorescence Decay Data Analysis. Analysis of fluorescence decay data was performed using the software DAS6.2 (JobinYvon, Edison, NJ). The analysis is carried out by assuming that the fluorescence experimental decay profile, $R(t)$, is the convolution between the true fluorescence decay, $I(t)$, and the prompt, $G(t)$, according to the equation

$$R(t) = \int_0^t G(t - t')\, I(t')\, \mathrm{d}t' \tag{4}$$

where $I(t)$ is of the form

$$I(t) = \sum_i \alpha_i \mathrm{e}^{-t/\tau_i} \tag{5}$$

with α_i being the relative amplitude of the component with lifetime τ_i. The algorithm fits, using the least-squares method, the experimental decay, $R(t)$, by convoluting the experimentally recorded $G(t)$ with the theoretical function $I(t)$. The fitting minimizes the reduced χ^2 while varying α_i and τ_i. The quality of the fitting was judged by the value of χ^2, the visual inspection of the residual, and the value of the Durbin−Watson factor[42] which is an indicator of the autocorrelation of the residuals. The lifetime data discussed in the Results section includes only fitting that yielded a value of $\chi^2 < 1.60$ and a Durbin−Watson factor in the 1.8−2.0 range. Fittings of the fluorescence decays were carried out with up to four exponential components. The retrieval of α_i and τ_i was used to form a detailed description of the contribution of the two Trp residues to BLGA fluorescence.

In addition, the value of τ_i and the average lifetime, $\langle\tau\rangle$, defined as

$$\langle\tau\rangle = \sum_i \alpha_i \tau_i \tag{6}$$

were used to calculate the bimolecular quenching rate, k_q, from the value of the slope, K, of the S−V plots[40]

$$k_q = \frac{K}{\tau} \tag{7}$$

Fluorescence decay curves were also collected as a function of the emission wavelength at steps of 5 nm in the 300−380 nm range.

Results

pH Dependence of the Steady-State Fluorescence of BLGA and NATA. Because BLGA undergoes a significant pH-dependent conformational change, we analyzed its intrinsic fluorescence in the pH range 5−9 and compared it with the fluorescence of NATA.

After normalization for absorption, the emission intensity and the position of the emission maximum of BLGA (333−334 nm) and NATA (350−351 nm) remained approximately constant at all pHs. Also, after normalization for the absorption, the fluorescence properties of BLGA (intensity and position of the maximum) are identical between excitation at 280 and 295 nm.

pH Dependence of the Fluorescence Lifetime of BLGA and NATA. *BLGA.* The fluorescence lifetime measurements of the protein show that the decay is slower at higher pH (Figure 2A). Under our experimental conditions, the decays are best fitted by three-exponential components ($\chi^2 < 1.35$); however, below pH 7, the contribution of the very short-lived component is near the resolution limit of our instrument (estimated at approximately 250 ps), as demonstrated by the large relative error on the data point (Table 1). When factored into the average lifetime (eq 6), the contribution of this short-lived component is nearly negligible (<2%). At pH 7 and above, however, the short component becomes more easily resolved ($\tau > 0.5$ ns) and contributes more to the overall fluorescence (∼5%). The intermediate fluorescence lifetime (τ_2) does not vary significantly upon increasing the pH from 5 to 9, showing only a 12% increase from pH 7 to pH 9. Conversely, the longer fluorescence lifetime (τ_3) depends strongly on the pH of the solution (Table 1 and Figure 2C). At pH 5 (well below the conformational transition of BLGA), this component is 2.38 ± 0.39 ns and increases up to 4.33 ± 0.46 ns at pH 9 where previous data[15,43] predict that the pH-dependent conformational transition of BLGA is completed while the pH-dependent unfolding of the protein has not occurred yet. The relative amplitude of the intermediate component remains basically constant, while the longer-lived component decreases as an effect of the increase of the short (sub-nanosecond) component at pH 7, 8, and 9 (Table 1 and Figure 2B). The pH-dependent fluorescence decay produces a constant increase of the average decay lifetime (Table 1).

NATA. The fluorescence decay of NATA was best fitted by a monoexponential decay as reported by other authors.[41] The single lifetime is virtually constant within the pH range investigated (2.95 ± 0.03 ns).

Dependence on Emission Wavelength. The fluorescence decay of BLGA depends on the emission wavelength, as shown in Figure 3. At all pHs investigated, the fluorescence decay is "slower" at longer wavelengths (Figure 3A and B). A closer inspection shows that at all pH values the short and intermediate lifetimes remain constant (Figure 3D and Table 2), the relative contribution of each component (α_i) also remains virtually constant (Figure 3C), and only the longer-lived component increases its lifetime at longer wavelengths (Figure 3D and Table 2). The relative increase of τ_3 is larger at smaller pH values (51% at pH 5, 28% at pH 9). The average lifetime also increases

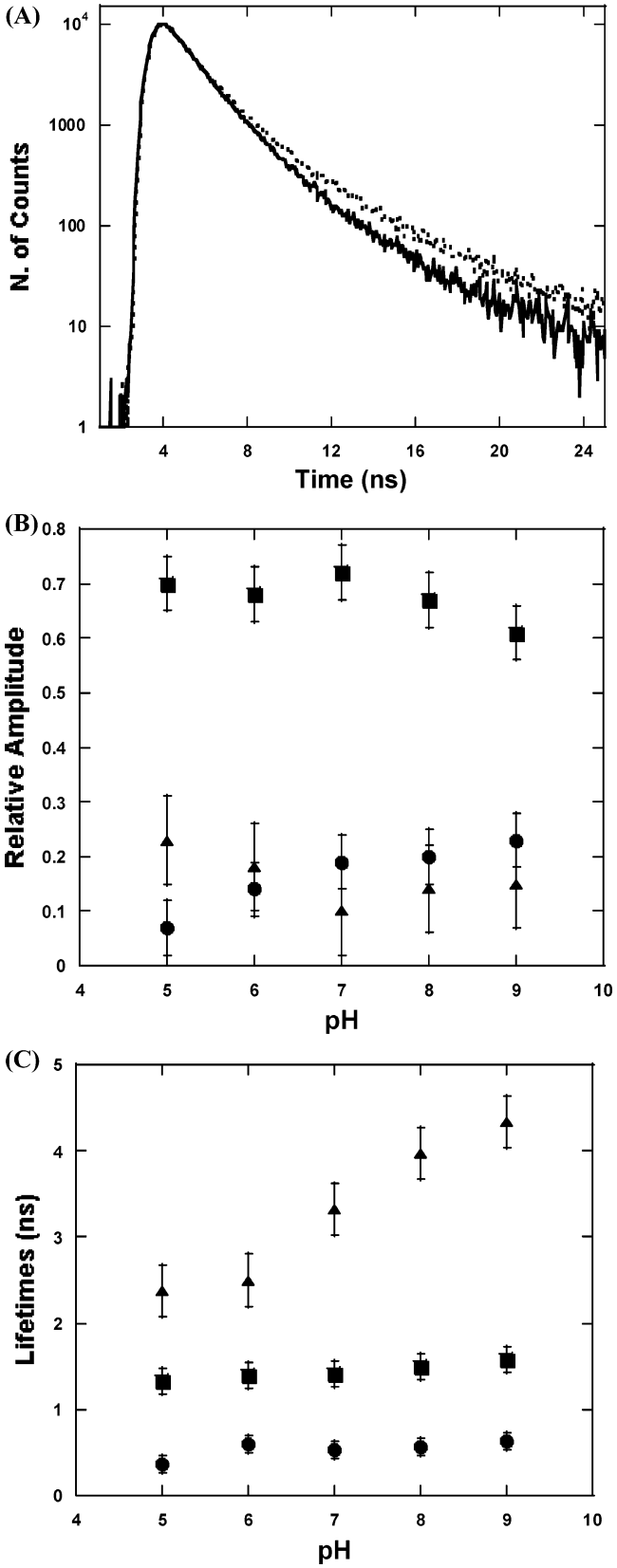

Figure 2. (A) Fluorescence decay of BLGA at pH 5 (solid) and pH 9 (dotted). $\lambda_{em} = 330 \pm 2$ nm. (B) Relative amplitudes of the decay components as a function of pH: α_1 (circles); α_2 (squares); α_3 (triangles). (C) Lifetimes of the three fluorescence decay components as a function of pH: τ_1 (circles); τ_2 (squares); τ_3 (triangles). The data points were obtained from the average of the three runs.

TABLE 1: Fluorescence Lifetime Components of BLG[a]

pH	α_1	τ_1	α_2	τ_2	α_3	τ_3	$\langle\tau\rangle$	χ^2
5	0.07 ± 0.03	0.37 ± 0.19	0.70 ± 0.08	1.33 ± 0.10	0.23 ± 0.13	2.38 ± 0.39	1.48 ± 0.11	1.04 ± 0.06
6	0.04 ± 0.01	0.47 ± 0.12	0.78 ± 0.07	1.41 ± 0.18	0.28 ± 0.13	2.50 ± 0.27	1.55 ± 0.13	1.03 ± 0.05
7	0.1 ± 0.05	0.54 ± 0.17	0.72 ± 0.04	1.40 ± 0.18	0.18 ± 0.08	3.33 ± 0.66	1.66 ± 0.23	1.13 ± 0.10
8	0.20 ± 0.07	0.56 ± 0.37	0.67 ± 0.04	1.49 ± 0.18	0.14 ± 0.04	3.97 ± 0.63	1.67 ± 0.21	1.08 ± 0.08
9	0.23 ± 0.05	0.64 ± 0.04	0.61 ± 0.04	1.58 ± 0.17	0.15 ± 0.03	4.33 ± 0.46	1.76 ± 0.43	1.06 ± 0.04

[a] ±, standard deviation.

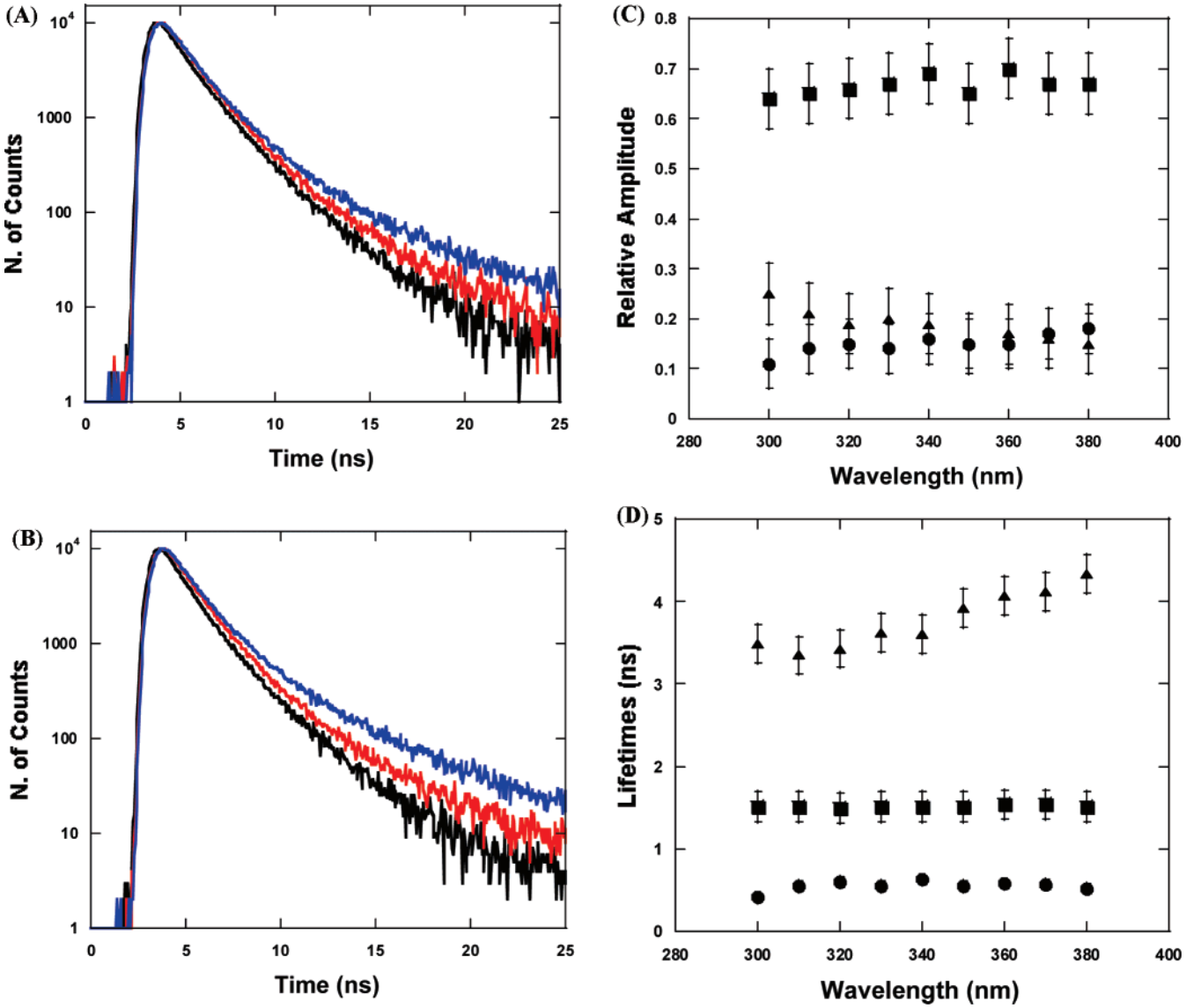

Figure 3. (A) Fluorescence decay curves of BLGA as a function of emission wavelength at pH 5 (λ_{em} = 310 nm (black), 330 nm (red), and 380 nm (blue)). (B) Fluorescence decay curves of BLGA as a function of emission wavelength at pH 9 (λ_{em} = 310 nm (black), 330 nm (red), and 380 nm (blue)). (C) Relative amplitude of the decays at pH 9 as a function of emission wavelength: α_1 (circles); α_2 (squares); α_3 (triangles). (D) Fluorescence lifetimes of the decays at pH 9 as a function of emission wavelength: τ_1 (circles); τ_2 (squares); τ_3 (triangles). All of the figures qualitatively represent the trend at other pH values as detailed in Table 2.

with the emission wavelength (Table 2 and Figure 4). Interestingly the relative increase (~30%) is basically constant at all pH values.

Unlike BLGA decay, NATA fluorescence lifetime does not depend on the emission wavelength (data not shown).

Steady-State Fluorescence of BLGA and NATA in the Presence of Urea. *BLGA.* As reported by others,[3,5] the addition of urea to the solutions containing BLGA produces a red shift of the emission maximum and an increase of the fluorescence intensity. The rate of the shift of the emission is pH-dependent. For pH < 8, at 1 M urea, the maximum still occurred at 330 nm; however, at an identical concentration of urea but for pH 8 and 9, the emission maxima were already shifted to 335 nm (Figure 5A). As the pH of the solution increased, the shift appeared at lower urea concentration so that at pH 5 the maximum emission wavelength of 350 nm occurred at 7 M, while at pH 9 it occurred at 5 M. The maxima of the emission spectra reached 350 ± 1 nm at 8 M for all pHs (Figure 5A). The sigmoidal increase of fluorescence intensity (Figure 4B) is well documented, although our study is the first to investigate it in such a wide range of pH. The fluorescence increase is opposite to the decrease expected from the exposure to the

TABLE 2: Dependence of Fluorescence Lifetime upon Emission Wavelength[a]

pH	λ_{em}	α_1	τ_1 (ns)	a_2	τ_2 (ns)	α_3	τ_3 (ns)	$\langle\tau\rangle$ (ns)	χ^2
5	310	0.06	0.35	0.68	1.22	0.28	2.21	1.47	1.14
	330	0.07	0.37	0.70	1.33	0.23	2.55	1.54	1.07
	350	0.04	0.36	0.71	1.34	0.27	2.45	1.63	1.05
	380	0.05	0.61	0.69	1.35	0.26	3.35	1.83	1.07
6	310	0.12	0.49	0.68	1.34	0.20	2.20	1.41	1.16
	330	0.14	0.60	0.68	1.40	0.18	2.50	1.49	1.01
	350	0.11	0.57	0.77	1.40	0.12	2.79	1.48	1.11
	380	0.09	0.49	0.77	1.39	0.14	3.32	1.58	1.12
7	310	0.24	0.58	0.69	1.40	0.07	3.01	1.32	1.19
	330	0.19	0.54	0.72	1.40	0.18	3.17	1.68	1.12
	350	0.21	0.63	0.72	1.42	0.07	3.83	1.42	1.20
	380	0.21	0.61	0.71	1.46	0.08	4.49	1.52	1.10
8	310	0.21	0.55	0.65	1.51	0.14	3.35	1.57	1.12
	330	0.20	0.56	0.67	1.50	0.14	3.44	1.60	1.17
	350	0.15	0.55	0.70	1.51	0.15	3.92	1.73	1.14
	380	0.15	0.52	0.67	1.51	0.18	4.34	1.87	1.08
9	310	0.27	0.63	0.58	1.59	0.14	3.63	1.60	1.04
	330	0.23	0.63	0.61	1.58	0.15	4.33	1.76	1.11
	350	0.23	0.66	0.60	1.55	0.17	4.28	1.82	1.17
	380	0.19	0.63	0.59	1.59	0.22	4.65	2.08	1.15

[a] Standard deviation similar to the one in Table 1.

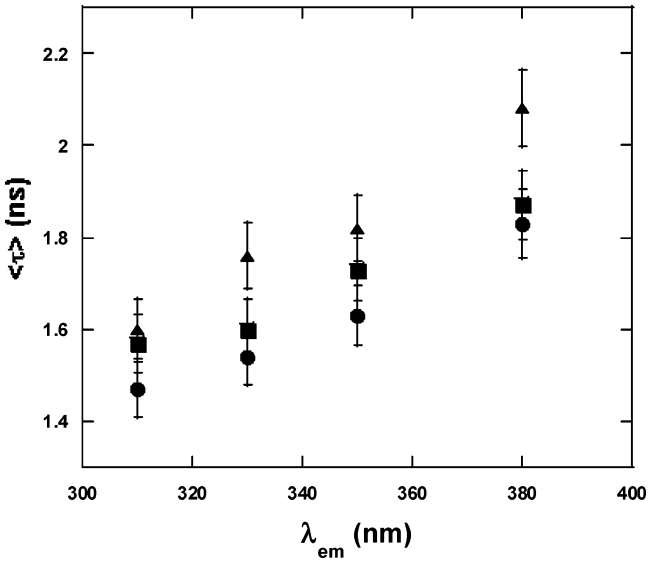

Figure 4. Average fluorescence lifetime (eq 6) as a function of the emission wavelength, λ_{em}: pH 5 (circles); pH 8 (squares); pH 9 (triangles).

aqueous solvent of previously buried (or partially buried) Trp residues.[41] The increase of protein fluorescence upon unfolding is not unprecedented and in other cases was used to separate the contribution of different Trp residues in a multi-Trp protein.[44] At lower pH, an intermediate plateau seems to occur. The plateau appears between 4 and 5 M urea at pH 5 and between 3 and 4 M urea at pH 7. At pH 8 and 9, instead, the intermediate plateau disappeared (Figure 5B). Assuming the DCU model described previously, the steady-state fluorescence data can be used to determine the free energy associated with the urea-induced unfolding at different pH according to eq 2 (Figure 6). The free energy data are summarized in Table 3 and show that BLG is more stable to urea denaturation at lower pH (especially below the conformational transition). At low pH (<8), the comparison between the two-state model and the DCU yields very different values of *m*. At pH 8 and 9, however, the values of *m* obtained via the DCU or the TS analysis (second and fourth columns of Table 3) are nearly identical. This was not directly observed before; however, it was speculated that the DCU model would work well in the range of pH between 3.5 and 7.4.[5] At

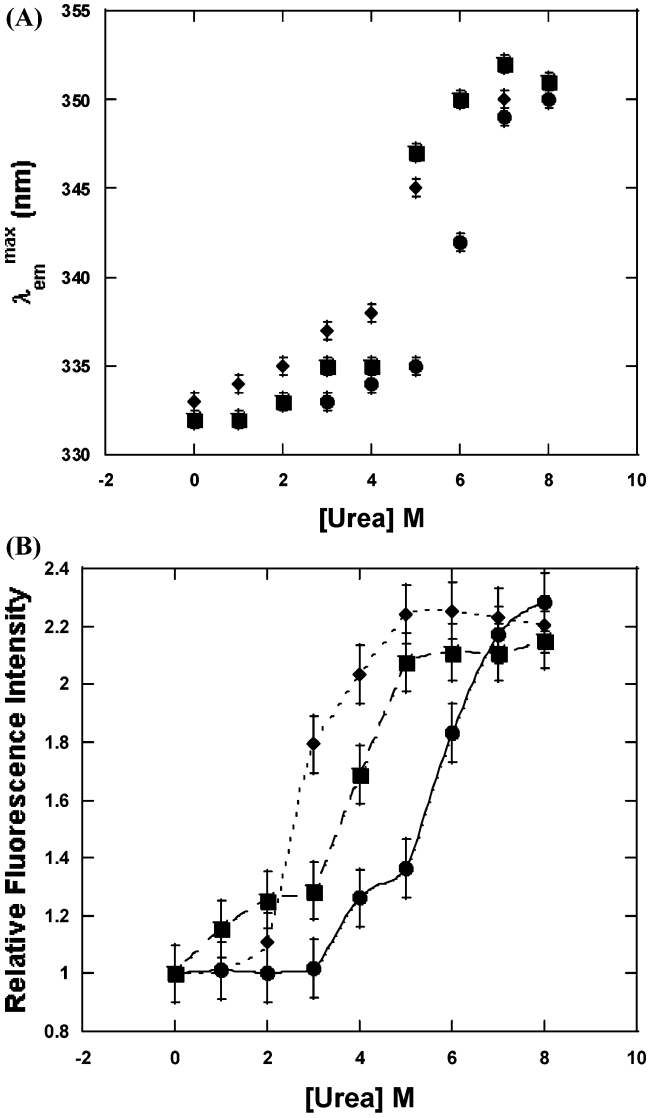

Figure 5. (A) Position of the emission maximum of BLGA as a function of urea. (B) Fluorescence intensity of BLGA, normalized for the absorption, as a function of urea concentration: pH 5 (circles); pH 7 (squares); pH 9 (diamonds).

all pH values, $\Delta G°$ calculated with the DCU model is much higher than the one calculated with the two-state model; however, the energy retrieved by the DCU model is in agreement with most published data, whereas the two-state model appears to underestimate the energy associated with the denaturation process.

Fluorescence Decay of BLG and NATA in the Presence of Urea. *BLGA.* The fluorescence decay of BLGA is strongly affected by the presence of urea at all pH values (Figure 7). Since urea produces a shift of the emission maximum, the values of the decay parameters were compared to those obtained in native BLGA at the corresponding emission wavelength (Table 2). The average lifetime for the decays shows a sigmoidal increment which is reminiscent of the one observed for the intensity. However, the details of Table 4 suggest three scenarios depending on the pH of the solution and the concentration of urea:

(1) Within a certain urea concentration, the decay parameters retain values similar to the ones obtained for native BLGA at the respective pH values. At pH > 7, the range of urea concentration (0−3 M) where the native properties of BLGA are maintained is smaller than that at lower pH (0−5 M). This

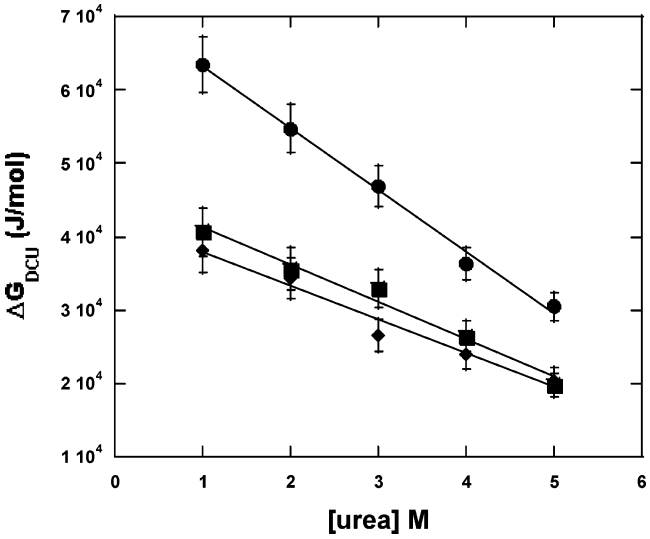

Figure 6. Linear dependence of the free energy of unfolding, $\Delta G°$, as a function of urea concentration according to the DCU model, using eq 2: pH 5 (circles); pH 7 (squares); pH 9 (diamonds).

TABLE 3: Unfolding Parameters for BLGA in Urea Using the DCU and the Two-State Model[a]

pH	m_{DCU}[b] ((kJ/mol)·(1/M))	$\Delta G°_{DCU}$ (kJ/mol)	m_{TS}[c] ((kJ/mol)·(1/M))	$\Delta G°_{TS}$ (kJ/mol)
5	7.22 ± 0.91	68.4 ± 6.5	4.04 ± 0.37	22.1 ± 3.3
6	4.44 ± 0.63	51.5 ± 5.1	2.68 ± 0.08	14.6 ± 0.9
7	2.86 ± 0.40	38.0 ± 4.3	2.33 ± 0.07	6.68 ± 1.3
8	2.79 ± 0.27	34.8 ± 4.5	2.34 ± 0.27	4.30 ± 0.9
9	2.53 ± 0.22	35.8 ± 5.0	2.39 ± 0.22	7.19 ± 5.0

[a] ±, standard deviation. [b] DCU, dissociation coupled unfolding. [c] TS, two-state unfolding..

is in agreement with the native or quasi-native steady-state emission spectra in the same range of urea concentration.

(2) Beyond the urea concentrations discussed above, the three-exponential decay still fits the decay adequately but with a different set of parameters. At all pH values, the sub-nanosecond component disappears and in its place a lifetime with 3.3 ns < τ < 3.9 ns appears with a relative amplitude which increases with urea. The intermediate component maintains a native value for the lifetime, but its relative amplitude decreases with urea. The longer component, however, becomes extremely long-lived (τ > 6.3 ns and often >10 ns) and its relative amplitude reduces to 0.1 or less.

(3) Because of the unusually large (for Trp) τ_3 obtained in some of the three-exponential fits (Table 4), we attempted to add a fourth component to the fitting. Because of the nature of the fitting procedure, a fourth component is normally not justified unless one or more of the lifetimes are fixed. Under the assumption that Trp19 is the major chromophore in native BLGA, a four-component fitting was carried out by fixing the values of τ_2 to its initial values obtained for the corresponding emission wavelength. Fixing τ_2 is preferable to fixing τ_3 because it does not depend on the emission wavelength (Table 2). As expected, the additional component improved the value of χ^2 (<1.2) and the value of the Durbin−Watson parameter (1.85−1.95). With four-component fitting, the sub-nanosecond component (τ_1) is maintained with a relative amplitude that decreases at increasing urea concentration and tends to become negligible. τ_3 increases to values above 3 ns, and a fourth component with a lifetime fluctuating between 5.5 and 8 ns (depending on the pH) appears. The relative amplitude of τ_3 increases to become dominant (>45%), while the relative amplitude of the longer-lived component (τ_4) also increases (Table 4).

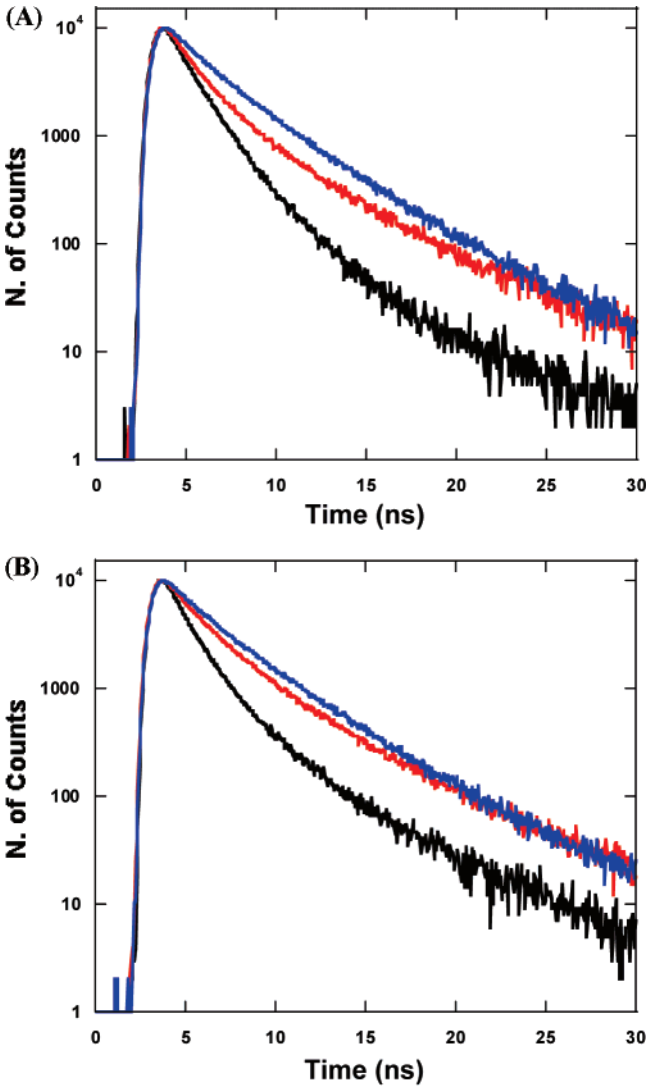

Figure 7. Fluorescence decay curves of BLGA at different concentrations of urea: (A) pH 5; (B) pH 9. 0 M urea (black), 4 M urea (red), 8 M urea (blue).

We propose that this uncertainty in the number of components to the fitting is directly correlated with the "unquenching" of Trp61 which occurs at higher urea concentration at all pH values (see the Discussion). Additional components, due to Trp61, with lifetimes near those of Trp19 would create problems due to the resolution properties of the fitting.

NATA. The fluorescence decay of NATA remains monoexponential at all urea concentrations and pH values and increases slightly from 2.95 ± 0.03 to 3.22 ± 0.1 ns regardless of the pH of the solution (data not shown).

Quenching by KI and Acrylamide. *Steady-State Fluorescence*. Overall, the fluorescence of BLGA was not quenched by KI up to a concentration of 0.5 M, whereas acrylamide quenched BLGA fluorescence with a large quenching constant (~8.6 M^{-1}) (Figure 8A). The quenching constant did not vary substantially with the pH, leading to a bimolecular constant (eq 7) of 6.61 × 10^9 M^{-1} s^{-1} at pH 5 and 5.47 × 10^9 M^{-1} s^{-1} at pH 9. The quenching analyzed with Stern−Volmer showed that after the initial linear portion the quenching proceeded with an upward curvature (data not shown).

Fluorescence Lifetime. In agreement with the steady-state measurements, the decay of BLGA fluorescence shows that the addition of KI does not produce any substantial change in the fluorescence decay parameters, whereas the addition of acry-

TABLE 4: Dependence of Fluorescence Lifetime upon Urea Concentration[a]

[urea] (M)	α_1	τ_1 (ns)	α_2	τ_2 (ns)	α_3	τ_3 (ns)	α_4	τ_4 (ns)	χ^2	D−W[b]
					pH 5					
1	0.10	0.48	0.75	1.34	0.17	2.71			1.13	1.91
2	0.09	0.50	0.74	1.33	0.18	2.85			1.08	1.86
3	0.08	0.52	0.75	1.34	0.18	2.64			1.19	1.92
4	0.11	0.44	0.76	1.36	0.14	3.44			1.07	1.88
5	0.15	0.58	0.75	1.34	0.10	3.53			1.14	1.90
6	0.55	3.67	0.40	1.34	0.05	6.53			1.13	2.10
	0.13	*0.74*	*0.08*	*1.34*	*0.52*	*2.53*	*0.26*	*4.33*	*1.11*	*1.89*
7	0.69	3.58	0.23	1.34	0.06	6.51			1.14	1.96
	0.05	*0.44*	*0.09*	*1.34*	*0.39*	*2.45*	*0.47*	*4.43*	*1.10*	*1.87*
8	0.67	3.38	0.22	1.34	0.11	6.28			1.19	1.81
	0.04	*0.43*	*0.08*	*1.34*	*0.43*	*2.45*	*0.45*	*4.51*	*1.12*	*1.85*
					pH 7					
1	0.19	0.51	0.72	1.42	0.12	3.88			1.22	1.94
2	0.18	0.58	0.69	1.51	0.14	4.19			1.04	1.87
3	0.10	0.42	0.66	1.42	0.24	4.28			1.18	1.88
4	0.06	0.28	0.58	1.42	0.37	4.38			1.19	1.89
5	0.58	3.67	0.33	1.42	0.10	7.51			1.21	1.85
	0.14	0.44	0.21	1.42	0.54	3.25	0.21	4.10	1.15	1.88
6	0.70	3.71	0.26	1.45	0.04	8.07			1.12	1.90
	0.06	0.34	0.56	1.48	0.67	3.67	0.08	4.60	1.09	1.88
7	0.67	3.83	0.28	1.49	0.03	8.60			1.15	1.84
	0.04	0.33	0.26	1.48	0.67	3.83	0.03	*4.80*	1.12	1.89
8	0.69	3.67	0.23	1.42	0.08	6.38			1.17	2.04
	0.03	0.33	0.26	1.45	0.68	3.83	0.04	4.68	1.13	1.99
					pH 9					
1	0.22	0.62	0.63	1.59	0.21	4.41			1.12	1.88
2	0.17	0.59	0.55	1.77	0.29	4.12			1.15	1.89
3	0.06	0.35	0.47	1.60	0.48	4.71			1.34	1.57
4	0.52	4.14	0.44	1.59	0.04	10.32			1.22	1.93
	0.08	*0.50*	*0.12*	*1.58*	*0.53*	*2.82*	*0.22*	*4.15*	*1.23*	*1.88*
5	0.59	4.12	0.37	1.65	0.04	12.4			1.14	1.94
	0.12	*0.85*	*0.04*	*1.59*	*0.64*	*2.87*	*0.23*	*4.15*	*1.17*	*1.86*
6	0.62	3.83	0.37	1.62	0.01	10.9			1.33	2.03
	0.08	*0.62*	*0.12*	*1.61*	*0.50*	*3.77*	*0.31*	*4.41*	*1.18*	*1.89*
7	0.60	3.90	0.34	1.63	0.06	8.90			1.50	1.62
	0.10	*0.81*	*0.15*	*1.64*	*0.40*	*3.89*	*0.36*	*4.46*	*1.21*	*1.80*
8	0.66	3.83	0.31	1.62	0.07	7.03			1.37	1.50
	0.08	*0.77*	*0.17*	*1.62*	*0.46*	*3.98*	*0.29*	*4.92*	*1.14*	*2.00*

[a] Standard deviation similar to the one in Table 1. [b] Durbin−Watson Factor.

lamide decreases both τ_1 and τ_2 without altering their respective relative amplitudes. The summary of some of the fluorescence decay parameters is shown in Table 5. From the right-hand side of eq 1, we could obtain the S−V and bimolecular quenching constant for each individual component. This led us to establish that the component of τ_2 is quenched more efficiently than the component relative to τ_3 at al pH values (Table 6). If one compares the values of Table 6 with those of Table 5, it is apparent that the quenching parameters are instead pH-dependent, as k_q decreases for both components of the decay at increasing pH. This is consistent with a less buried environment of the emitting Trp residue at higher pH values. It also shows that the steady-state fluorescence overestimates (larger k_q) the purely collisional quenching, indicating some static component of acrylamide quenching, as suggested by others.[24]

Collisional quenching[40] by acrylamide, a neutral quencher, rather than KI, an ionic quencher, suggests that the quenching occurs at a mostly buried location.

Discussion

Structural X-ray models[15,16] suggest that the pH-dependent conformational transition of BLGA involves portions and groups of the protein that are distant from both Trp residues. This is confirmed by the negligible changes of the steady-state emission of BLG in the 5−9 pH range.

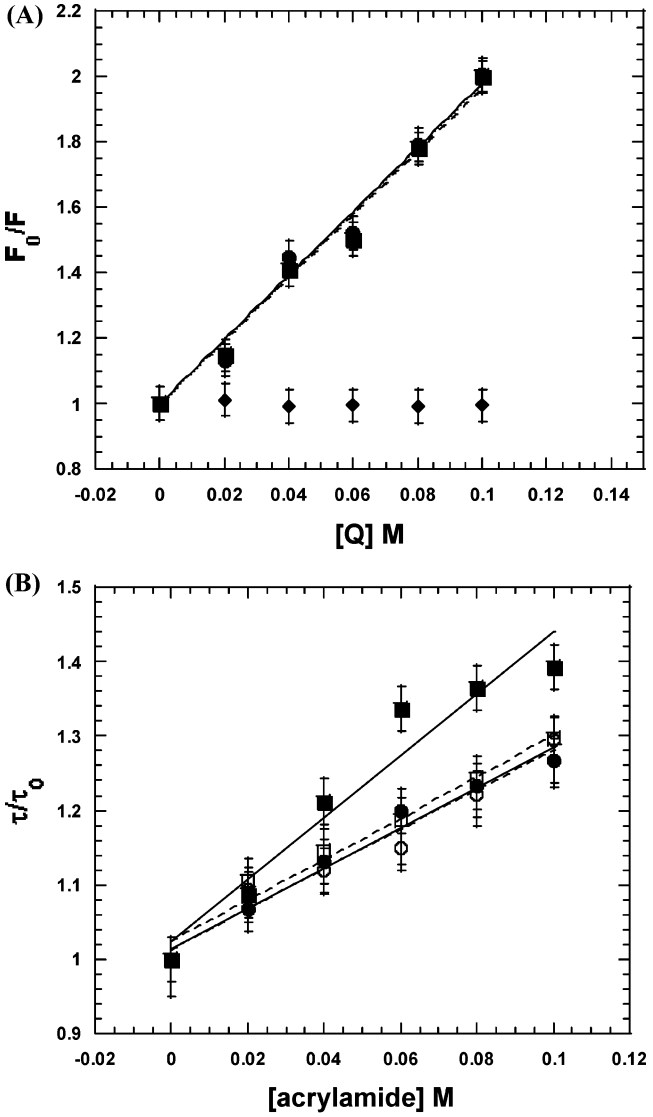

Figure 8. (A) Stern−Volmer plot of BLGA quenching using the overall intensity: quenching by acrylamide at pH 5 (circles); quenching by acrylamide at pH 9 (squares); quenching by KI at pH 7 (diamonds). The quenching of KI yielded similar results at all pH values. (B) Stern−Volmer plot of BLGA quenching by acrylamide using the fluorescence lifetimes: filled circles (τ_2, pH 5); filled squares (τ_3, pH 5); hollow circles (τ_2, pH 9); hollow squares (τ_3, pH 9).

Conversely, the fluorescence lifetime data suggest a different scenario. The longer-lived lifetime (τ_3), and to a much lesser extent τ_2, increase from pH 5 to pH 9 (Table 1 and Figure 2C). This suggests that smaller changes, below the detection limit of X-ray diffraction experiments, may occur in the proximity of at least one of the Trp residues. Since BLGA has two Trp residues (Figure 1), we first need to establish which residue probes the pH-induced structural changes. Although previous studies reported different interpretations of BLGA intrinsic fluorescence,[6,24,31] we believe that the work of Cho et al.[8] unequivocally showed that Trp19 is the only contributor to native BLGA fluorescence, indirectly proving that Trp61 is strongly quenched by the proximal Cys66−Cys160 disulfide bond (Figure 1C). Disulfide moieties have been shown to strongly quench Trp residues in proteins.[45,46] A survey of available BLG structures reveals that the distance between Trp61 and the S−S bond is 3.5−4.5 Å (Figure 1B) which is well below

TABLE 5: Representative Examples of Fluorescence Decay of BLGA as a Function of KI and Acrylamide[a]

[Q] (M)	α_1	τ_1 (ns)	α_2	τ_2 (ns)	α_3	τ_3 (ns)
			KI (pH 7)			
0	0.12	0.70	0.70	1.40	0.18	3.33
0.02	0.11	0.65	0.70	1.42	0.19	3.75
0.06	0.13	0.57	0.71	1.40	0.17	3.39
0.10	0.10	0.54	0.70	1.40	0.20	3.27
			KI (pH 9)			
0	0.23	0.64	0.61	1.58	0.15	4.33
0.02	0.24	0.61	0.64	1.51	0.12	4.27
0.06	0.27	0.60	0.61	1.54	0.12	4.28
0.10	0.18	0.58	0.66	1.57	0.16	4.15
			Acrylamide (pH 5)			
0	0.07	0.37	0.70	1.33	0.23	2.38
0.02	0.06	0.40	0.67	1.14	0.27	1.85
0.06	0.15	0.56	0.76	1.11	0.09	1.78
0.10	0.09	0.40	0.67	1.05	0.24	1.71
			Acrylamide (pH 9)			
0	0.23	0.64	0.61	1.58	0.15	4.33
0.02	0.25	0.52	0.63	1.55	0.12	3.92
0.06	0.19	0.42	0.68	1.43	0.13	3.65
0.10	0.23	0.51	0.64	1.22	0.13	3.34

[a] Standard deviation similar to the one in Table 1.

TABLE 6: Quenching Parameters Obtained from Steady-State as Well as Time-Resolved Emission of BLGA

	steady-state emission		fluorescence lifetime			
pH	K_{S-V} (M^{-1})	K_q (M^{-1} s^{-1})	$K_{S-V}(\tau_2)$ (M^{-1})	$K_q(\tau_2)$ (M^{-1} s^{-1})	$K_{S-V}(\tau_3)$ (M^{-1})	$K_q(\tau_3)$ (M^{-1} s^{-1})
5	9.57	6.61×10^9	2.85	2.17×10^9	4.37	1.84×10^9
6	9.42	6.48×10^9	3.56	2.54×10^9	2.68	1.09×10^9
7	9.55	6.17×10^9	2.38	2.02×10^9	5.27	1.79×10^9
8	9.42	5.78×10^9	1.18	1.87×10^9	2.38	0.76×10^9
9	9.60	5.47×10^9	2.88	1.82×10^9	3.07	0.70×10^9

the critical quenching distance of 7 Å.[47] Also, a substantial contribution of an exposed indole residue such as Trp61 would shift the emission maximum to longer wavelengths.

The sole contribution of Trp19 to the fluorescence of native BLGA is confirmed by our quenching investigations. The quenching by acrylamide, and the absence of quenching by KI, is in agreement with what has been reported by others.[3,17,24] Trp19, being buried, is more likely quenched by a neutral molecule such as acrylamide than an ionic quencher such as I^-. The quenching of acrylamide shows that both τ_2 and τ_3 components are affected (Table 5 and Figure 8). Considering (i) the data of Cho et al.[8] and (ii) the acrylamide dependence of the fluorescence lifetime, we conclude that the components associated with τ_2 and τ_3 are both associated with Trp19. This conclusion is somewhat in agreement with what was observed by Portugal et al.[24] Nonetheless, where they resolved a very short lifetime (<0.15 ns), which is beyond our resolution, while we resolved an intermediate lifetime (1.3−1.6 ns) which they did not resolve. They too observed a quenching of the longer lifetime, and they could also observe the quenching of another sub-nanosecond lifetime, corresponding to our τ_1, whose quenching we could not observe because of the time resolution of our instrument. Also, we could not detect the transient, acrylamide-induced unquenching of BLGA fluorescence.[24]

Thus, under native conditions, BLGA fluorescence is dominated by Trp19 which is associated with at least two lifetimes (τ_2 and τ_3) in the 1−4 ns region. The assignment of the sub-nanosecond component is instead less clear because its lifetime is at the very limit of our instrument resolution.

Our fluorescence data open new questions. Trp19 is located in a buried position at the bottom of the β-barrel of the protein.[15,16] Nonetheless, the pH dependence (Table 1 and Figure 2) and the emission wavelength dependence (Table 2 and Figure 3) of the fluorescence lifetime are typical of a Trp residue located in a more polar environment.[38,41] According to X-ray data, the bottom of the barrel of BLGA, where Trp19 is located, does not undergo any major or minor pH-dependent conformational change[15] and the effects of denaturants in this region are still unclear. Most of the amino acid residues in this region have average X-ray B-factors in the 20−40 range. Trp19 has a B-factor of 25.5 ± 8.1 which indicates some residual mobility.

How can the structural data be reconciled with our fluorescence data? Why does Trp19 of native BLGA decay with a multiexponential function (Table 1)? Why does Trp19 fluorescence depend on the pH of the solution? And, finally, why does the fluorescence decay of BLGA show an emission-dependent behavior?

The multiexponentiality of Trp19 has been attributed to the classic rotamer model,[24,39,48] but X-ray data on BLG do not show any variable or alternative conformation of Trp19 which instead appears to be in a very constrained environment.[14−16,29,49] This situation, for other proteins, has been discussed extensively by Dahms et al.,[39] who reached the conclusion that rotamers do exist in crystallized proteins but they may be too difficult to resolve by X-ray under most circumstances. Moreover, in the case of BLGA, the relative amplitude of one lifetime (∼60−70%) is much larger than the other (15−25%) which suggests that one rotamer is dominant and would probably correspond to the usual conformation of Trp19 that is retrieved from the various structures of BLG deposited at the Protein Data Bank.

The existence of rotamers of Trp19 generating different contributions to the fluorescence decay offers a way to rationalize our results.

The emission wavelength dependence of Trp residues (Table 2 and Figure 3) is typical of a "polar" environment which would create inhomogeneous excited states dependent upon the reorganization of the polar environment around the excited indole.[38] Such relaxation produces lower energy states and occurs in the time scale of the fluorescence decay, thus making these lower energy states detectable at longer times and wavelengths.[38] Table 2 shows that the longer-lived component, with smaller relative amplitude, is affected. Thus, we can conclude that the rotamer corresponding to τ_3 is in a more polar environment then the dominant rotamer, τ_1, which is not affected by the emission wavelength. This is surprising considering the buried location of Trp19. However, it is likely that the less populated rotamers are configured in such a way as to either increase exposure with the region outside the pocket or form hydrogen bonds between the indole group and other groups in its proximity. A survey of the available 3D structures of BLGA offers some explanations. Despite the apparent hydrophobic location, Trp 19 is actually in proximity of charged groups such as Lys14, Lys100, and Arg124 (Figure 8B). Lys14 and Lys100 are at a distance of 12.5 ± 1.2 and 11.4 ± 1.9 Å, respectively, from the indole ring of Trp19; such a distance is too large to form hydrogen bonds (HBs) but could provide a more polar local environment for Trp19 especially if the less populated Trp19 rotamer locates close enough to one of the residues. Despite these considerations which we cannot entirely rule out, Arg124 offers the more likely candidate to create the polar microenvironment of Trp19 for the following reasons: (i) the distance between Arg124 and the indole ring of Trp19 is 3.48 ± 0.8 Å (Figure 9), thus much closer than Lys14 or Lys100, (ii) it has been shown that Arg residues have a stronger interaction with indole rings[34] than Lys residues, and (iii) the

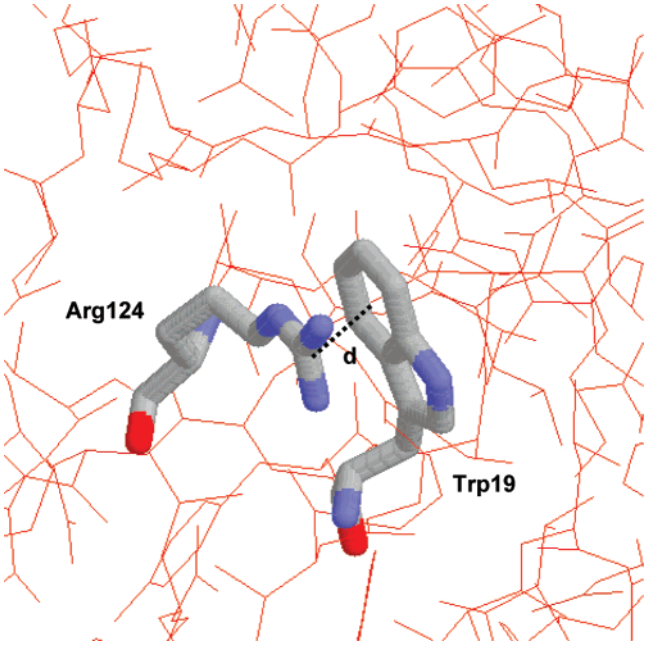

Figure 9. Representation, in CPK color scheme, of the proximity between Arg124 and Trp19. The distance **d** between the positively charged region of Arg and the benzene portion of the indole ring is 3.48 ± 0.8 Å.

positively charged group of Arg124 is on the side of the benzene ring of the indole. It is well-established that, of the two lowest excited electronic states,[33,37] ^1L_a is the one responsible for most Trp fluorescence.[37] This state is associated with a configuration where the electron density is shifted to the benzene portion of the indole ring.[37] Thus, a positively charged group would more favorably interact with the ^1L_a state when located on the benzene side of the indole ring. Arg124 could in fact provide three possible mechanisms that would explain the increased polarity of the Trp19 environment: (i) the charge on the Arg side chain produces a polar environment near the indole ring, (ii) one of the NH groups on the Arg side chain forms a HB with the indole ring,[34,50] or (iii) the interaction occurs through a NH$-\pi$ bond with the indole ring.[34,35,37] These interactions are obviously larger for the less populated Trp19 rotamer and would explain the existence of time-dependent lower energy excited states (Table 2). Such a rotamer also probes pH changes, even though it is far from the major structural modifications occurring in the protein structure. The lesser, but still evident, dependence of τ_2 upon the pH value (Table 1) is also in agreement with this interpretation, since Arg124 is close to Trp19 in every crystallographic configuration surveyed and could provide a polar surrounding to the main rotamer of Trp19.

Changes in pH could modify the charge of Arg124 and/or the charge of some of the Lys residues in a Lys-rich region of the protein. Although the pK_a value of buried Arg has a wide variability,[51,52] it has been reported that in many situations it can be as low as 7.5.[53] This effect could also be modulated by the proximity of several Lys residues whose pK_a might also be lower when buried in the interior of a protein. Thus, Trp19 could probe the titration of the Arg124 residues which is its most proximal amino acid in the BLGA structure.[34,37]

In addition, in other lipocalins, the region outside the calyx on the side of the three-turn α-helix is more flexible (Mazzini, A. et al. Private communication). This, in combination with the higher reactivity of Cys121 at alkaline pH,[19,23] seems to indicate that in solution the protein may undergo some substantial changes that modify the region near Trp19.

Since mainly τ_3 is sensitive to the pH changes, the modification of the BLGA conformation near Trp19 affects the lesser populated rotamer more than the dominant rotamer (τ_2), which likely is the one observed by X-ray. These changes, however, are significant enough to affect the indole moiety, if this is either closer to the outside of the β-barrel or in proximity of amino acids (such as Arg124) which are probably modified by the increase in pH.

Finally, our study provides some interesting observation for the probing of the unfolding of BLGA. The increase of BLGA fluorescence with increasing concentration of urea has been reported before[3,17] and is in agreement with the unquenching of Trp61. Under conditions where BLG is partly denatured by urea, this could occur because Trp61 distances itself from the disulfide moiety and/or because the Cys66−Cys160 bond breaks upon denaturation due to the increased distance between the two Cys residues. The urea dependence of the fluorescence decay could suggest this latter scenario. Upon fitting with three-exponential decays, the sub-nanosecond lifetime is replaced, at all pH values, by a longer-lived component whose lifetime is 3.76 ± 0.18 ns and does not appear to be pH-dependent (Table 4). The four-exponential fitting (Table 4) also shows that a component with approximately the same lifetime becomes dominant as the concentration of urea increases. Thus, we suggest that this lifetime can be attributed to the contribution of the unquenched Trp61. At wavelengths in the 340−350 nm range where the unfolding BLGA has maximum fluorescence, this contribution becomes indistinguishable with the wavelength-dependent contribution of native τ_3 (Table 2) so that one component of Trp19 and Trp61 may lead to similar emission lifetimes.

The transient plateau observed at lower pH values using steady-state fluorescence (Figure 5) may suggest the detection of monomerization of BLGA in agreement with the DCU model. However, the fluorescence lifetime experiments did not yield any additional information on this process (Table 4). Monomerization of BLGA would mainly affect Trp61 which participates in the dimer formation.[16,20,54] This reinforces the hypothesis that Trp61 is indeed "silent" in the native monomer and would not yield any information regarding the monomerization of the protein. The energy data retrieved through Figure 6 indicate a less stable structure of BLGA dimers at higher pH, already suggested by others[5,17] and consistent with the pI of BLGA,[9] where the unfolding would instead occur before or concomitantly with the monomerization.

In summary:

(a) Our results show that the fluorescence of Trp19 is consistent with the existence of two rotamers (at least), one which is dominant and is engaged in mostly hydrophobic interaction with its neighboring amino acids and another that interacts with a more polar environment likely through interactions with the proximal Arg124 residue. This second rotamer has a behavior typical of more exposed Trp residues, as the fluorescence lifetime depends on the emission wavelength.

(b) The rotamer associated with τ_3 (Table 1) probes the pH dependence of BLGA conformation because of (i) the proximity to pH-sensitive Lys and Arg residues and (ii) the possible mobility of the region of the three-turn α-helix which at higher pH could undergo a substantial conformational change in solution and increase the polarity of the environment around Trp19.

(c) Finally, our study indicates that the fluorescence lifetime of the unquenched Trp61 (in the presence of urea) is in the

3.5−3.8 ns region. To our knowledge, the contribution of this chromophore to the fluorescence decay has not been reported before.

Although our model is satisfying, we are undertaking investigations where the theoretical model of the Trp rotamer distribution in BLGA will be compared to the fluorescence lifetime.

Acknowledgment. The authors would like to thank Dr. David A. Wampler and Dr. Donald Kurz (Department of Chemistry, UTSA) for their help in establishing the purity of BLGA with HPLC and SDS-PAGE. The study was in part funded by the UTSA Faculty Research Award.

References and Notes

(1) Katakura, Y.; Totsuka, M.; Ametani, A.; Kaminogawa, S. *Biochim. Biophys. Acta* **1994**, *1207*, 58.
(2) Renard, D.; Lefebvre, J.; Griffin, M. C. A.; Griffin, W. G. *Int. J. Biol. Macromol.* **1998**, *22*, 41.
(3) Creamer, L. K. *Biochemistry* **1995**, *34*, 7170.
(4) Qi, X. L.; Holt, C.; McNulty, D.; Clarke, D. T.; Brownlow, S.; Jones, G. R. *Biochem. J.* **1997**, *324*, 341.
(5) Galani, D.; Apenten, R. K. O. *Food Res. Int.* **1999**, *32*, 93.
(6) D'Alfonso, L.; Collini, M.; Baldini, G. *Biochemistry* **2002**, *41*, 326.
(7) Blanch, E. W.; Hecht, L.; Barron, L. D. *Protein Sci.* **1999**, *8*, 1362.
(8) Cho, Y.; Batt, C. A.; Sawyer, L. *J. Biol. Chem.* **1994**, *269*, 11102.
(9) Collini, M.; D'Alfonso, L.; Baldini, G. *Protein Sci.* **2000**, *9*, 1968.
(10) D'Alfonso, L.; Collini, M.; Baldini, G. *Biochim. Biophys. Acta* **1999**, *1432*, 194.
(11) Lange, D. C.; Kothari, R.; Patel, R. C.; Patel, S. C. *Biophys. Chem.* **1998**, *74*, 45.
(12) Marden, M. C.; Dufour, E.; Christova, P.; Huang, Y.; Leclerc-L'Hostis, E.; Haertle, T. *Arch. Biochem. Biophys.* **1994**, *311*, 258.
(13) Tian, F.; Johnson, K.; Lesar, A. E.; Moseley, H.; Ferguson, J.; Samuel, I. D. W.; Mazzini, A.; Brancaleon, L. *Biochim. Biophys. Acta* **2005**, *1760*, 38.
(14) Kontopidis, G.; Holt, C.; Sawyer, L. *J. Mol. Biol.* **2002**, *318*, 1043.
(15) Qin, B. Y.; Bewley, M. C.; Creamer, L. K.; Baker, H. M.; Baker, E. N.; Jameson, G. B. *Biochemistry* **1998**, *37*, 14014.
(16) Brownlow, S.; Morais Cabral, J. H.; Cooper, R.; Flower, D. R.; Yewdall, S. J.; Polikarpov, I.; North, A. C. T.; Sawyer, L. *Structure* **1997**, *5*, 481.
(17) Busti, P.; Scarpeci, S.; Gatti, C.; DeLorenzi, N. *Food Res. Int.* **2002**, *35*, 871.
(18) Gasymov, O. K.; Abduragimov, A. R.; Yusifov, T. N.; Glasgow, B. J. *Biochemistry* **2002**, *41*, 8837.
(19) Crougennec, T.; Molle, D.; Mehra, R.; Bouhallab, S. *Protein Sci.* **2004**, *13*, 1340.
(20) Fessas, D.; Iametti, S.; Schiraldi, A.; Bonomi, F. *Eur. J. Biochem.* **2001**, *268*, 5439.
(21) Dong, A.; Matsuura, J.; Allison, S. D.; Chrisman, E.; Manning, M. C.; Carpenter, J. F. *Biochemistry* **1996**, *35*, 1450.
(22) Vetri, V.; Militello, V. *Biophys. Chem.* **2005**, *113*, 83.
(23) Hoffmann, M. A. M.; van Mil, P. J. J. M. *J. Agric. Food Chem.* **1997**, *45*, 2942.
(24) Portugal, C. A. M.; Crespo, J. G.; Lima, J. C. *J. Photochem. Photobiol., B* **2006**, *82*, 117.
(25) Kundu, S.; Melton, J. S.; Sorensen, D. C.; Phillips, G. N. *Biophys. J.* **2002**, *83*, 723.
(26) Smith, D. K.; Radivojac, P.; Obradovic, Z.; Dunker, A. K.; Zhu, G. *Protein Sci.* **2003**, *12*, 1060.
(27) Radivojac, P.; Obradovic, Z.; Smith, D. K.; Zhu, G.; Vucetic, S.; Brown, C. J.; Lawson, J. D.; Dunker, A. K. *Protein Sci.* **2004**, *13*, 71.
(28) Yuan, Z.; Bailey, T. L.; Teasdale, R. D. *Proteins* **2005**, *58*, 905.
(29) Qin, B. Y.; Creamer, L. K.; Baker, E. N.; Jameson, G. B. *FEBS Lett.* **1998**, *438*, 272.
(30) Qi, X. L.; Brownlow, S.; Holt, C.; Sellers, P. *Biochim. Biophys. Acta* **1995**, *1248*, 43.
(31) Dufour, E.; Marden, M. C.; Haertle, T. *FEBS Lett.* **1990**, *277*, 223.
(32) Gasymov, O. K.; Abduragimov, A. R.; Yusifov, T. N.; Glasgow, B. J. *Biochim. Biophys. Acta* **1999**, *1433*, 307.
(33) Weber, G. *Biochem. J.* **1960**, *75*, 335.
(34) Samanta, U.; Pal, D.; Chakrabarti, P. *Proteins* **2000**, *38*, 288.
(35) Nanda, V.; Brand, L. *Proteins* **2000**, *40*, 112.
(36) Hennecke, J.; Sillen, A.; Huber-Wunderlich, M.; Engelborghs, Y.; Glockshuber, R. *Biochemistry* **1997**, *36*, 6391.
(37) Vivian, J. T.; Callis, P. R. *Biophys. J.* **2001**, *80*, 2093.
(38) Lakowicz, J. R. *Photochem. Photobiol.* **2000**, *72*, 421.
(39) Dahms, T. E. S.; Willis, K. J.; Szabo, A. G. *J. Am. Chem. Soc.* **1995**, *117*, 2321.
(40) Eftink, M. R.; Ghiron, C. A. *Anal. Biochem.* **1981**, *114*, 189.
(41) Eftink, M. R. *Biophys. J.* **1994**, *66*, 482.
(42) Durbin, J.; Watson, G. S. *Biometrika* **1951**, *38*, 159.
(43) Tanford, C.; Bunville, L. G.; Nozaki, Y. *J. Am. Chem. Soc.* **1959**, *81*, 4032.
(44) Knutson, J. R.; Walbridge, D. G.; Brand, L. *Biochemistry* **1982**, *21*, 4671.
(45) Ross, J. B. A.; Schmidt, C. J.; Brand, L. *Biochemistry* **1981**, *20*, 4369.
(46) Merola, F.; Rigler, R.; Holmgren, A.; Brochon, J. C. *Biochemistry* **1989**, *28*, 3383.
(47) Tanaka, F.; Kaneda, N.; Mataga, N.; Tamai, N.; Yamazaki, I.; Hayashi, K. *J. Phys. Chem.* **1987**, *91*, 6344.
(48) Szabo, A. G.; Rayner, D. M. *J. Am. Chem. Soc.* **1980**, *102*, 554.
(49) Kuwata, K.; Hoshino, M.; Forge, V.; Era, S.; Batt, C. A.; Goto, Y. *Protein Sci.* **1999**, *8*, 2541.
(50) Koenig, S.; Muller, L.; Smith, D. K. *Chem.—Eur. J.* **2001**, *7*, 979.
(51) Fukamizo, T.; Juffer, A. H.; Voge, H. J.; Honda, Y.; Tremblay, H.; Boucher, I.; Neugebauer, W. A.; Brzezinski, R. *J. Biol. Chem.* **2000**, *275*, 25633−25640.
(52) Berkovitch, F.; Nicolet, Y.; Wan, J. T.; Jarrett, J. T.; Drennan, C. L. *Science* **2004**, *303*, 76.
(53) Kim, J.; Mao, J.; Gunner, M. R. *J. Mol. Biol.* **2005**, *348*, 1283−1298.
(54) Uhrinova, S.; Smith, M. H.; Jameson, G. B.; Uhrin, D.; Sawyer, L.; Barlow, P. N. *Biochemistry* **2000**, *39*, 3565.